Planar waveguide LED illuminator with controlled directionality and divergence

William M. Mellette,* Glenn M. Schuster, and Joseph E. Ford

Department of Electrical and Computer Engineering, University of California San Diego, 9500 Gilman Drive, La Jolla, California 92093-0407, USA
wmellett@ucsd.edu

Abstract: We present a versatile illumination system where white light emitting diodes are coupled through a planar waveguide to periodically patterned extraction features at the focal plane of a two dimensional lenslet array. Adjusting the position of the lenslet array allows control over both the directionality and divergence of the emitted beam. We describe an analytic design process, and show optimal designs can achieve high luminous emittance ($1.3x10^4$ lux) over a 2x2 foot aperture with over 75% optical efficiency while simultaneously allowing beam steering over ± 60° and divergence control from ± 5° to fully hemispherical output. Finally, we present experimental results of a prototype system which validate the design model.

OCIS codes: (080.0080) Geometric optics; (110.2945) Illumination design; (080.4295) Nonimaging optical systems; (080.2175) Etendue; (230.7400) Waveguides, slab.

References and links

1. J.-G. Chang and Y.-B. Fang, "Dot-pattern design of a light guide in an edge-lit backlight using a regional partition approach," Opt. Eng. **46**(4), 10984–10995 (2012).
2. D. Feng, Y. Yan, X. Yang, G. Jin, and S. Fan, "Novel integrated light-guide plates for liquid crystal display backlight," J. Opt. A Pure Appl. Opt. **7**(3), 111–117 (2005).
3. T. C. Teng and J. C. Ke, "A novel optical film to provide a highly collimated planar light source," Opt. Express **21**(18), 21444–21455 (2013).
4. J. H. Karp, E. J. Tremblay, and J. E. Ford, "Planar micro-optic solar concentrator," Opt. Express **18**(2), 1122–1133 (2010).
5. J. M. Hallas, K. A. Baker, J. H. Karp, E. J. Tremblay, and J. E. Ford, "Two-axis solar tracking accomplished through small lateral translations," Appl. Opt. **51**(25), 6117–6124 (2012).
6. A. W. Lohmann, "Scaling laws for lens systems," Appl. Opt. **28**(23), 4996–4998 (1989).
7. D. T. Moore, G. R. Schmidt, and B. L. Unger, "Concentrated photovoltaic stepped planar light guide," in *International Optical Design Conference*, Technical Digest (Optical Society of America, 2010), paper JMB46P.
8. J. K. Kim, T. Gessmann, H. Luo, and E. F. Schubert, "GaInN light emitting diodes with RuO_2/SiO_2/Ag omni-directional reflector," Appl. Phys. Lett. **84**(22), 4508–4510 (2004).
9. H. Luo, J. K. Kim, E. F. Schubert, J. Cho, C. Sone, and Y. Park, "Analysis of high-power packages for phosphor-based white-light-emitting diodes," Appl. Phys. Lett. **86**(24), 243505 (2005).
10. H. J. Cornelissen, H. Ma, C. Ho, M. Li, and C. Mu, "Compact collimators for high brightness blue LEDs using dielectric multilayers," Proc. SPIE **8123**, 81230J (2011).
11. T.-C. Teng, W.-S. Sun, L.-W. Tseng, and W.-C. Chang, "A slim apparatus of transferring discrete LEDs' light into an ultra-collimated planar light source," Opt. Express **21**(22), 26972–26982 (2013).
12. R. Winston, J. C. Minano, and P. Benitez, *Nonimaging Optics* (Academic, 2005).
13. F. Fournier, W. J. Cassarly, and J. P. Rolland, "Method to improve spatial uniformity with lightpipes," Opt. Lett. **33**(11), 1165–1167 (2008).
14. M. Heiblum and J. H. Harris, "Analysis of curved optical waveguides by conformal transformation," IEEE J. Quantum Electron. **11**(2), 75–83 (1975).
15. S. Garner, H. Fong, M. He, P. Cimo, X. Li, Y. Cai, S. Ouyang, Y. Xie, Q. Shi, and S. Cai, "Flexible glass substrates for display and lighting applications," in *IEEE Photonics Conference (IPC)* (2013), pp. 176–177.
16. K. A. Denault, M. Cantore, S. Nakamura, S. P. DenBaars, and R. Seshadri, "Efficient and stable laser-driven white lighting," AIP Adv. **3**(7), 072107 (2013).
17. A. O. Marcano, C. Loper, and N. Melikechi, "High-sensitivity absorption measurement in water and glass samples using a mode-mismatched pump-probe thermal lens method," Appl. Phys. Lett. **78**(22), 3415–3417 (2001).
18. P. S. Chechurov and G. E. Romanova, "Using the ZEMAX software complex to form photometric models of LED illuminator devices," J. Opt. Technol. **79**(5), 302–304 (2012).

#203337 - $15.00 USD Received 19 Dec 2013; revised 27 Feb 2014; accepted 15 Mar 2014; published 1 Apr 2014

1. Introduction

Conventional illumination systems are typically designed to provide either directional or diffuse illumination, spot or flood lighting, using a fixed optical path through collimating or diffusing optics. In settings where the required type of illumination varies, light energy could be used more efficiently if the source could adapt to provide illumination consistent with the user's immediate need. For example, in home or office lighting the user may want to switch between directional task lighting to illuminate a workspace and diffuse lighting to illuminate an entire room.

Backlights for liquid crystal displays use waveguide illumination, varying the size and shape of features patterned on the light guide plate to control light extraction uniformity [1], and using optical sheets above the light guide to control the directionality of emitted light [2,3]. Control over directionality allows the display to preferentially direct light into a viewing cone. This viewing cone is fixed, however, because the optical components are designed to provide a single luminance distribution regardless of their relative positioning. Light cannot be actively directed toward an observer moving relative to the device.

Previous work on planar solar concentrators has demonstrated efficient, high-concentration designs that use a two dimensional lens array positioned above a micro-patterned waveguide [4]. The addition of a moveable lens array above the waveguide allows the concentrator to adapt to changing sun angle [5]. The same physical structure can be adapted for a versatile illuminator by reversing the direction of light propagation, and re-optimizing the design for the light source and output constraints.

Figure 1 shows an illustration of the system in which light emitting diodes (LEDs) are coupled to a planar multimode waveguide such that light is confined by total internal reflection (TIR) defined by Snell's law. As light propagates, it is scattered out of confined modes by periodic extraction features and subsequently interacts with the corresponding lens array, which directs the extracted light toward the target.

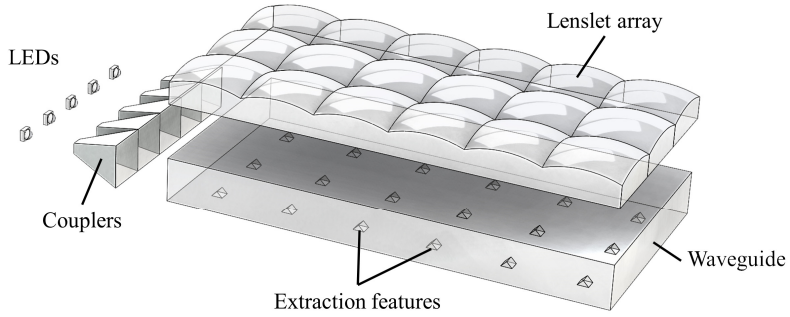

Fig. 1. Conceptual illustration of the planar illumination system. The components have been exploded for clarity.

Aligning the lenslet and extraction arrays with the extraction features located at or near the focal plane of the lenses produces a collimated output beam [Fig. 2(a)]. Laterally translating the lens array relative to the extraction array steers the overall beam by steering all individual beams in the same direction, as shown in Fig. 2(b). Relative rotations between the two arrays alter the overall divergence of the beam by steering the individual beams in a 'spiral' of different directions, as shown in Fig. 2(c). In Fig. 2 the divergence angle of the light extracted from the waveguide has been restricted, because lateral offsets between the arrays would otherwise induce unwanted crosstalk as light spills into adjacent lenses. This crosstalk leads to side lobes in the emitted pattern, which are undesireable for most applications.

#203337 - $15.00 USD Received 19 Dec 2013; revised 27 Feb 2014; accepted 15 Mar 2014; published 1 Apr 2014

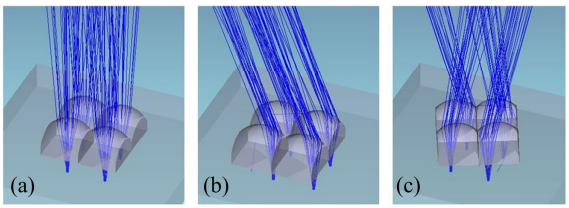

Fig. 2. Section of the array showing a collimated beam when the arrays are aligned (a), a redirected beam when the arrays are translated (b), and a diverging beam when the arrays are rotated (c).

The same functionality can be achieved using an array of point-like LED sources directly behind the lens array, which would eliminate the complexity of edge coupling and waveguiding. However, a waveguide-based design has the advantages that it 1) allows a thinner form factor and simplifies electrical routing and heat sinking by moving the LED sources to the edges of the waveguide; 2) clears the aperture opposite to the lens array from LEDs, wiring, and heat sinks, allowing the use of higher performing reflective lenses, discussed in Section 2.1; and 3) allows the coupling, waveguiding, and extraction structures to perform the necessary angular and spatial mapping of the real sources into an effective array of point-like sources. While the efficacy (electrical to luminous conversion efficiency) and emittance (spatial power density) of LED dies typically scale inversely with die size within one class of LEDs, so-called 'high power' LEDs with apertures larger than 2mm currently have higher performance in terms of emittance than do small package LEDs with apertures less than 1mm. From conservation of radiance, edge coupling a smaller number of high power LEDs will produce a brighter beam than a large number of small LEDs located directly behind the lens array. This edge coupling approach will be adaptable as LED technology improves, up to the point when the emittance of small aperture LEDs matches that of large aperture LEDs, which would warrant the direct array approach.

The thin form factor of the planar illuminator allows conformal mounting to flat surfaces with little or no recessing, making it ideal for retrofitting ceiling fixtures. Further, control over light from a relatively large aperture can be achieved with relatively short range mechanical motion compared to traditional designs. Control over a similar amount of light energy would require an array of traditional luminaires, with each element having its own actuation mechanism. Conventional actuation mechanisms require motion in 3 dimensions, either by moving a lens with radial and axial freedom with respect to the source or by gross actuation of the entire luminaire including the source and heat sink. The planar illuminator uses precise short-range 2D motion of one optical component to achieve the same degree of control.

In the following section we will present an analytic model of each element of the system, then in Section 3 combine the elements to obtain an overall system model, and determine the potential performance of optimal designs. In Section 4 we describe an experimental full-scale 'proof of principal' prototype, and compare its performance to the model. We conclude in Section 5 with some comments on future directions of this technology.

2. System design

Typical performance metrics for illumination systems include optical efficiency, efficacy, luminous emittance, and pattern uniformity. In our system, we are also concerned with the beam steering and divergence ranges conditional on the degree of crosstalk between adjacent lenses. We would also like the system to scale efficiently to large aperture sizes for high flux applications. Here we describe a simple analytic model for each element of the system, beginning at the output where we discuss lens performance, then moving to waveguiding and extraction, and finishing with the source and coupling methods.

2.1 Beam steering and diverging

The maximum steering angle, minimum divergence angle, and degree of crosstalk of emitted light are driven by two parameters: the lenslet F/# (focal length over aperture diameter) and

#203337 - $15.00 USD Received 19 Dec 2013; revised 27 Feb 2014; accepted 15 Mar 2014; published 1 Apr 2014

the divergence of light exiting the waveguide. From geometrical optics, using the paraxial lens approximation, the maximum steering angle with zero geometrical crosstalk is given by:

$$\psi_{\max} = \sin^{-1}\left(n \sin\left(\tan^{-1}\left(\frac{1}{2(F/\#)} - \tan(\theta_2) \right) \right) \right), \quad (1)$$

where θ_2 is the half divergence angle of the effective source immersed in refractive index n. Maximizing the steering angle corresponds to minimizing the lens F/# and the divergence angle of the effective source. Also from geometrical optics, we can write the minimum divergence angle due to the spatial extent of the effective source as:

$$\varphi = \sin^{-1}\left(n \sin\left(\tan^{-1}\left(\frac{w_{facet}}{2f} \right) \right) \right), \quad (2)$$

where w_{facet} is the full width of the effective source and f is the focal length of the lens. For a small minimum divergence angle, corresponding to a tightly collimated output beam, the lateral extent of the source needs to be small with respect to the focal length of the lens.

In the waveguide solar concentrator, light illuminates the entire face of the lenslets and lenslet aberrations are a critical factor in design. However, for an illuminator it is not necessary to emit from the entire surface area, and illuminating only a fraction of the lens area can be useful to minimize lateral crosstalk [Fig. 3]. Lens aberrations affect the performance of the system to the extent that they increase beam divergence. Under-filled lenses contribute fewer aberrations because light only interacts with a localized section of the lens surface. Reflective plano-convex singlets produce lower F/#s than do refractive designs for the same radius of curvature and, consequently, can be driven to lower overall F/#s [5]. Fresnel lenses are a viable option to reduce the F/# of refractive lenses while simultaneously reducing weight, but low F/# Fresnel lenses typically have poor off-axis performance due to increased scatter from zone transitions. Shorter focal length lenses are desirable because aberrations scale with lens dimensions [6] and because they make the illumination pattern more uniform by the nature of having more lenses per unit area. In some designs, it may be beneficial to induce a small fixed defocus by tuning the axial height of the lens in order to blur or 'smooth out' any sharp features present in an otherwise perfectly imaged intensity distribution.

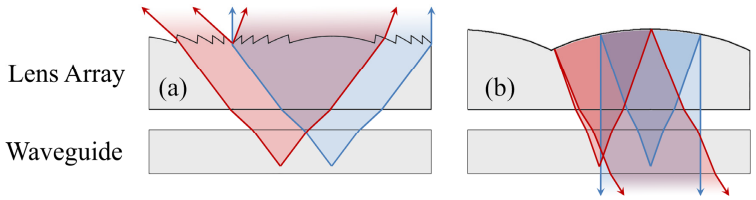

Fig. 3. Lens geometry examples: (a) fully filled refractive Fresnel lens showing crosstalk with lateral translation and (b) partially filled reflective spherical lens showing zero crosstalk with equivalent translation and F/#.

2.2 Light guiding and extraction

The extraction features act as the effective sources for the lenses by intercepting and redirecting light propagating in the waveguide toward the lens array. Light may be extracted from the waveguide using reflection, refraction, diffraction, or diffuse scattering. Flat faceted features are desirable because they have broadband performance (unlike dispersive gratings) and conserve angular divergence (unlike diffusers or curved facets). The conservation of angular divergence is crucial for minimizing crosstalk and generally keeps the system more étendue-limited, leading to more efficient designs.

#203337 - $15.00 USD Received 19 Dec 2013; revised 27 Feb 2014; accepted 15 Mar 2014; published 1 Apr 2014

The waveguide confines light by TIR for a sufficient angular spectrum, allowing light to be efficiently distributed to the extraction sites. The type of waveguide determines the relationship between the waveguide thickness and the dimensions of extraction features. We considered two waveguide designs. One is a constant cross section and 'constant mode volume' (CMV) waveguide [Fig. 4(a)] where light is shared between extraction sites, and the other is a laterally tapered 'stepped mode volume' (SMV) waveguide [Fig. 4(b)] where each extraction site adiabatically truncates the modal volume [7].

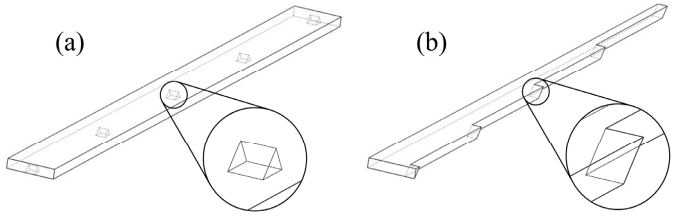

Fig. 4. Constant (a) and stepped (b) mode volume waveguide illustrations for N = 5 extraction sites. Each section as drawn supplies light to one row of lenses above the waveguide (not shown).

In the SMV design, light makes a single pass through the structure and is extracted uniformly up to a factor determined by the material's absorption coefficient. There is a fixed relationship between the facet and waveguide dimensions given by:

$$w_{facet} = \frac{t_{wg}}{\tan\gamma} = t_{wg}\Big|_{\gamma=45^\circ}, \tag{3}$$

where t_{wg} is the waveguide thickness and γ is the angle the facet makes with respect to the waveguide plane. Without loss of generality we set γ = 45°, corresponding to the case where the average direction of guided propagation is in the plane of the waveguide. Altering this γ will necessitate a split in the angular spectrum (e.g. ± 30° out-of-plane propagation), which does not increase the total radiance in the guide, makes confinement more difficult, and tends to require more complicated coupling structures. We should also note here that the stepped waveguide has a geometrical relationship limiting its length given the size and number of facets, as will be discussed in Section 3.2.

In the CMV geometry, light makes multiple passes through the waveguide and extraction is fundamentally non-uniform. We model the percentage of light energy extracted at a facet as the ratio between the facet cross section and the waveguide cross section. This model ignores shadowing effects, which is valid when the divergence is relatively large and the facets are relatively small with respect to their period. First, we determine the facet cross section 'σ_f,' which is the cross sectional area of the facet seen by the average waveguide mode. By the reasoning presented above for the SMV waveguide, we set the facet angle γ to 45°. Constraining the base dimensions of the facet to be square (w_{facet} x w_{facet}) to produce a symmetric beam using a rotationally symmetric lens, the facet cross section is just the product of the facet width and height, where the height is half the width: $\sigma_f\big|_{\gamma=45^\circ} = w_{facet}^2/2$. We then write the distributed absorption and extraction per lens aperture as:

$$\chi = \left(1 - \frac{\sigma_f}{t_{wg} D}\right)\exp(-\alpha D), \tag{4}$$

where D is the full lens aperture and α is the absorption coefficient of the waveguide material. Modifying the Beer-Lambert law, where j runs from 1 to N facets, the output power at the j^{th} facet is given by:

#203337 - $15.00 USD Received 19 Dec 2013; revised 27 Feb 2014; accepted 15 Mar 2014; published 1 Apr 2014

$$P_{ext,j} = P_0 \frac{\sigma_f}{t_{wg} D} \cdot \frac{\left(\chi^{j-1} + \eta_2 \chi^{2N-j}\right)}{\left(1 - \eta_1 \eta_2 \chi^{2N}\right)}, \tag{5}$$

where P_0 is the power coupled into the waveguide, η_2 and η_1 are the reflection efficiencies from the end of the waveguide and the source, respectively, and N is the total number of extraction sites in the section of waveguide. By symmetry, we consider a section of waveguide that is one lens aperture wide and half the total system aperture long, taking $\eta_2 = 1$ and $\eta_1 = \eta_{coupler}{}^2 R_{LED}$, where $\eta_{coupler}$ is the coupler efficiency (discussed in Section 2.3) and is modeled as being equivalent in both forward and reverse directions and R_{LED} is the percentage of light recycled by the LED. The incident light recycled by a typical die is about 50% [8] and the phosphor efficiency can be as high as 70% per pass [9]. The total recycling efficiency can be approximated by two passes through the phosphor and one reflection from the die, which gives 25% total recycling efficiency. The total extracted power can be determined by evaluating the sum:

$$P_{ext,total} = \sum_{j=1}^{N} P_{ext,j} = P_0 \frac{\sigma_f}{t_{wg} D(\chi - 1)} \cdot \frac{\left(\chi^N - 1\right)\left(1 + \eta_2 \chi^N\right)}{\left(1 - \eta_1 \eta_2 \chi^{2N}\right)}, \tag{6}$$

where we consider the term on the right hand side which scales the input power P_0 to be the average extraction efficiency 'η_{ext},' referred to later in Section 3. In the CMV geometry the relationship between waveguide and facet dimensions is:

$$w_{facet} < 2 t_{wg}, \tag{7}$$

for γ = 45° in order for the facet to fit within the waveguide. Here, unlike for the SMV waveguide, there is no fixed geometrical relationship between facet geometry, number of facets, and waveguide length.

Recalling from Eq. (2) that minimizing the divergence of emitted light corresponds to minimizing w_{facet}, we find that by the geometry of the SMV waveguide [Eq. (3)] and by the desire for high extraction efficiency in the CMV waveguide [Eq. (6)], we would like to minimize the waveguide thickness 't_{wg}' in both cases.

2.3 Light sources and couplers

White LEDs currently have superior luminance and efficacy compared to other broadband sources. From conservation of radiance, the brightness at the output of any passive optical system is limited by the brightness of the source. Consequently, LEDs with the highest luminance are desirable because they provide more optical power with the same étendue. These 'high power' LEDs have die sizes exceeding 2mm in width and typically obey Lambert's cosine law, leading us to calculate the fraction of Lambertian power in a beam of half angle θ_1 to be:

$$\eta_{beam} = \sin^2\left(\theta_1\right). \tag{8}$$

For example, a Lambertian emitter output clipped at θ_1 = ± 71.65° still contains 90% of the total power. Having such a clearly defined beam divergence simplifies étendue calculations.

From the above and per Sections 2.1 and 2.2, a high system performance requires coupling large sources with a high divergence angle to a relatively thin waveguide, while minimizing the divergence and maximizing the spatial power density of coupled light. For high optical efficiency the design must conserve étendue. Approaches to solving similar problems have recently been proposed [10,11]. Our approach was to first collimate the source, allowing a

#203337 - $15.00 USD Received 19 Dec 2013; revised 27 Feb 2014; accepted 15 Mar 2014; published 1 Apr 2014

tradeoff between divergence and spatial power density, and then perform a space-variant aperture transformation to interface with the thin waveguide.

The compound parabolic concentrator (CPC) is a standard nonimaging optical component that provides nearly étendue limited concentration and (path-reversed) collimation [Fig. 5, top row] [12]. However, any spatial nonuniformity in the collimated output intensity distribution reduces the uniformity of the waveguide illuminator output. Following previous work [13], we defined a CPC-like collimator with enhanced spatial uniformity at the output using quadratic Bezier curves [Fig. 5, bottom row].

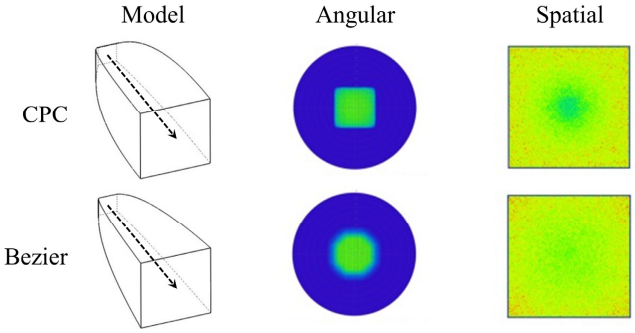

Fig. 5. Angular and spatial output distributions for a conventional CPC and a Bezier collimator both with a uniform Lambertian input.

To a high degree of accuracy, we can approximate both collimator designs as conserving étendue, so for two square apertures:

$$h_1 \sin(\theta_1) = h_2 \sin(\theta_2), \tag{9}$$

where h_1 and h_2 are the full widths of the source and exit apertures and θ_1 and θ_2 are the half divergence angles of light entering and exiting the collimator, respectively.

Next, we consider two designs to transform the exit aperture of the collimator to interface with the waveguide: 'faceted' and 'curled'. Both designs are variants of a stepped mode volume structure where the change in aspect ratio 'M' from collimator to waveguide is equal to the number of segments:

$$M = \frac{h_2}{t_{wg}}, \tag{10}$$

where, as in Eq. (9), h_2 is the full width of the output aperture of the collimator. The first design uses a series of flat reflective rectangular facets acting like fold mirrors to sequentially redirect segments of light exiting the collimator into the waveguide [Fig. 6(a)]. The structure was designed assuming perfectly collimated light and then analyzed in nonsequential Zemax to determine performance as a function of divergence [Fig. 6(b)]. A perfect aperture mapping can be achieved using two reflective facets per segment. Our final faceted design used a single facet per segment to reduce complexity and reflective surface loss, because this imperfect mapping approaches the ideal mapping as the aspect ratio M increases.

#203337 - $15.00 USD Received 19 Dec 2013; revised 27 Feb 2014; accepted 15 Mar 2014; published 1 Apr 2014

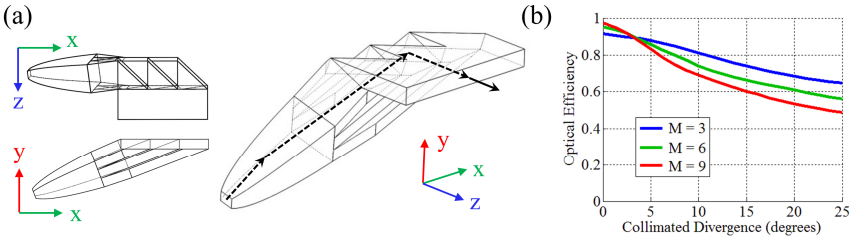

Fig. 6. Wireframe models of faceted coupler with M = 3 segments (a) and corresponding optical efficiency for M = 3, 6, and 9 segments (b).

The 'curled' coupler design we considered uses adiabatic light propagation through curved waveguide sections to 'strip' light energy and transform the aperture [Fig. 7(a)]. Following previous work on the confinement properties of curved multimode waveguides by conformal mapping [14], it can be shown that the half divergence angle ' θ_0 ' incurred from interaction with the curved structure is related to the thickness of the waveguide ' t ' and the outer bend radius ' R ' by:

$$\theta_0 = \cos^{-1}\left(1-\frac{t}{2R}\right). \tag{11}$$

For small ratios of t/R, the structure preserves étendue and has nearly equivalent confinement properties to a flat waveguide of the same refractive index. The blue curve in Fig. 7(b) for $t/R = 0.1$ has nearly 100% optical efficiency up to a half divergence angle of about 46°, compared to the 47.8° TIR angle corresponding to a flat guide with an equal index of 1.49. Unlike the faceted coupler, the optical efficiency of the curled structure is independent of the aspect ratio M. While the curled coupler outperforms the faceted design in terms of optical efficiency, it is less readily manufacturable. It is possible that advances in optical 3D printing technologies will enable inexpensive fabrication of such structures in the future. At present, flexible Corning Willowglass [15] presents a possible fabrication option.

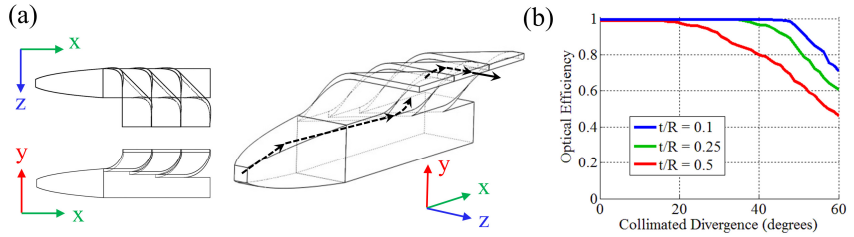

Fig. 7. Wireframe models of curled coupler showing 3 segments (a) and corresponding optical efficiency for a few ratios of t/R (b). The efficiency is independent of aspect ratio.

As the aspect ratio M increases, the 'staircase' shaped intermediate aperture in the faceted design [Fig. 6(a), shown with $M = 3$] approaches a square, as in the curled design [Fig. 7(a)], considerably simplifying the geometry. The efficiency and ease of manufacture of these couplers will increase as sources with higher luminance and smaller apertures become available through advances in LED technology or other alternatives [16].

3. System-level analytic model and optimization

System-level optimization of the planar illuminator is difficult in standard optical design software because of the complex geometries and merit functions. We developed an analytic model based on equations from imaging and nonimaging optics to give an intuitive optimization approach that provided more confidence than a 'black box' method. The designs resulting from the analytic optimization were modeled in Solidworks and ray traced with non-sequential Monte Carlo analysis using Zemax to insure the accuracy of the analytic model. A

#203337 - $15.00 USD Received 19 Dec 2013; revised 27 Feb 2014; accepted 15 Mar 2014; published 1 Apr 2014

truly ‘optimal’ solution is predicated on a detailed list of application-specific constraints and performance metrics. Without the information needed for a quantitative merit function, we optimized according to qualitative ideas of well-balanced performance.

We constrained certain aspects of the design space using parameters from commercially available LEDs and from a comparison lighting fixture. For a comparison fixture, we considered a 2x4 foot 3-tube fluorescent modular ceiling ‘troffer’ fixture with a luminous flux of 9000 lm, an efficacy of 92.19 lm/W, and an emittance of $1.475\text{x}10^4$ lux at the aperture. This gave us a target emittance value independent of system aperture size. We chose to set the system aperture to 2x2 feet with the intent of retrofit compatibility with modular ceiling grids. For the waveguide LED source we chose to use the Cree XLamp XM-L2, one of the highest luminous emittance and efficacy single-die LED sources available, delivering 728 lumens at 2A, 3V (about 2/3 max current) in a 2.5x2.5 mm die size. Low-loss BK7 glass was used for the waveguide for its low absorption coefficient of $3\text{x}10^{-4}$ m^{-1} [17].

From conservation of energy, we can relate the luminous emittance ‘ I_{out} ’ to the luminous flux of the LED ‘ P_{LED} ’ by:

$$I_{out} = \eta_{beam}(\theta_1)\eta_{coupler}(M,\theta_2)\eta_{ext}\left(\sigma_f, D, t_{wg}, N, \chi, \eta_1, \eta_2\right)\frac{t_{wg}\cos\theta}{NDh_2{}^2}P_{LED}, \quad (12)$$

where η_{ext} is the term that scales P_0 in the right hand side of Eq. (6) and θ is the step angle of the waveguide, as shown in Fig. 8. The second to last term in Eq. (12) encompasses the ratio between the output area of the coupler and the input area of the waveguide while scaling the output power by the output aperture to convert to emittance.

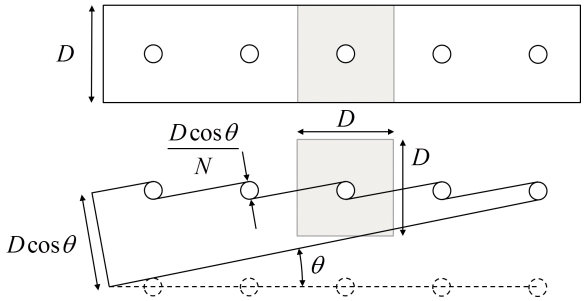

Fig. 8. Top down views of the CMV (top) and SMV (bottom) waveguides with N = 5 extraction sites. The grey squares indicate the position and size of a single lens.

In the subsequent sections, we consider designs that allow us to solve Eq. (12) and determine overall system performance. The first, using a constant mode volume waveguide and faceted light coupler (CMV-F), is chosen to provide the simplest path to manufacture. The second, using a stepped mode volume waveguide and curled coupler (SMV-C), is intended to enable the highest optical performance. We also briefly summarize a third design using a constant mode volume waveguide and curled coupler (CMV-C).

3.1 Design 1: constant mode volume with faceted coupler

The first design aims for manufacturability at the cost of performance by using the faceted coupling structure and a constant mode volume waveguide. The coupler is compatible with injection molding and the waveguide with roll processing of glass or plastic sheets.

First, we fit a parameterized 2 dimensional function to the simulated faceted coupler efficiency curves shown in Fig. 6(b). The mathematical form of the function was approximated from knowledge of the shape and boundary conditions of the simulated curves to be:

#203337 - $15.00 USD Received 19 Dec 2013; revised 27 Feb 2014; accepted 15 Mar 2014; published 1 Apr 2014

$$\eta_{coupler}\left(M,\theta_2\right)=\frac{f_1\left(M,\vec{A}_1\right)}{f_1\left(M,\vec{A}_2\right)\theta_2+f_1\left(M,\vec{A}_3\right)}+\frac{f_2\left(M,\vec{A}_4\right)}{\left(f_2\left(M,\vec{A}_5\right)\theta_2\right)^2+f_2\left(M,\vec{A}_6\right)}, \quad (13)$$

where:

$$f_1\left(M,\vec{A}_i\right)=A_{i,1}M^2+A_{i,2}M+A_{i,3}, \quad (14)$$

$$f_2\left(M,\vec{A}_i\right)=\frac{A_{i,1}}{A_{i,2}M+A_{i,3}}, \quad (15)$$

where the 3-element fit vectors $\vec{A}_1$ through $\vec{A}_6$ are determined by least squares minimization. The resulting parametric function is used in the optimization algorithm to give a predicted optical efficiency of the coupler in regimes that were not explicitly simulated beforehand.

From Eqs. (9) and (12), setting $\theta=0$ for the CMV waveguide geometry, we arrive at an implicit transcendental equation for θ_2:

$$\frac{h_1^2\sin^2\theta_1}{\sin^2\theta_2}=\eta_{beam}\left(\theta_1\right)\eta_{coupler}\left(M,\theta_2\right)\eta_{ext}\left(\sigma_f,D,t_{wg},N,\chi,\eta_1,\eta_2\right)\frac{t_{wg}P_{LED}}{I_{out}ND}, \quad (16)$$

where we recast $M=(h_1\sin\theta_1)/(t_{wg}\sin\theta_2)$ using Eqs. (9) and (10) so that the optimization problem is constrained to 4 dimensions: $\{t_{wg},\sigma_f,F/\#,N\}$, with the remaining variables fixed by design constraints. The optimization algorithm maps the design space by iterating through these 4 dimensions and numerically solving Eq. (16) over a grid of points in the space. For each point in $\{F/\#,N\}$ space, an optimal point in $\{t_{wg},\sigma_f\}$ space is found by maximizing a weighted sum of normalized maximum steering angle and normalized system efficiency [Fig. 9(a)]. The maximum steering angle is given by Eq. (1) and the overall optical system efficiency is the product of all efficiency terms in Eq. (16). We discarded solutions for which the minimum half divergence angle [Eq. (2)] is greater than a design limit of 5° and for which extraction deviation is greater than 1%, where the deviation is given by $\max_j\{|P_{ext,total}-NP_{ext,j}|/P_{ext,total}\}$ using Eqs. (5) and (6).

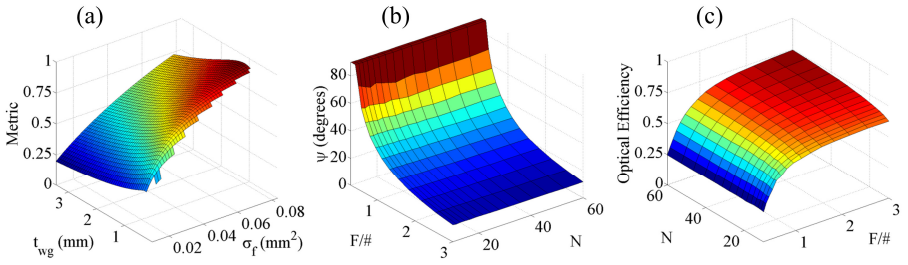

Fig. 9. CMV-F design space for 25% of target emittance. (a) Optimization metric for $N=60$, $F/\#=0.75$. (b) Maximum beam steering angle in $\{F/\#, N\}$ space. (c) Optical efficiency in $\{F/\#, N\}$ space. Note that the axes are rotated 90° counterclockwise from (b) to (c) to clearly illustrate the data.

Figures 9(b) and 9(c) show the corresponding optimums mapped from $\{t_{wg},\sigma_f\}$ to $\{F/\#,N\}$ space. There is a clear tradeoff between efficiency and maximum steering angle, which also depends on the target emittance. Higher emittance values drive both the maximum steering angle and efficiency down. High emittance requires a low aspect ratio M to maintain a high spatial power density, which either requires a thick waveguide or a small intermediate aperture [Eq. (10)]. To maintain the same minimum divergence angle for the same lens F/#

#203337 - $15.00 USD Received 19 Dec 2013; revised 27 Feb 2014; accepted 15 Mar 2014; published 1 Apr 2014

when the waveguide is made thicker, the facet dimension must be held constant [Eq. (2)], meaning the extraction efficiency decreases [Eq. (6)]. The other alternative, shrinking the intermediate aperture h_2, means that for the same beam efficiency [Eq. (8)], the divergence angle of coupled light increases [Eq. (9)], which both lowers the maximum steering angle [Eq. (1)] and lowers the coupler efficiency [Fig. 6]. Similar balancing forces are present when trying to push the maximum steering angle or the optical system efficiency as well.

Sweeping emittance values from 1 to 1/10 that of the target value ($1.475\text{x}10^4$ lux), we found that the performance metrics were balanced at about 1/4 of the reference emittance ($3.69\text{x}10^3$ lux). Using this value, we choose an 'optimal' faceted design with $N = 60$, $F/\# = 0.75$, $t_{wg} = 0.762$ mm, and $\sigma_f = 0.0762$ mm^2 [Fig. 10]. This design provided a good tradeoff between efficiency, steering angle, and emittance. Achieving such a low F/# required the use of a reflective lens array.

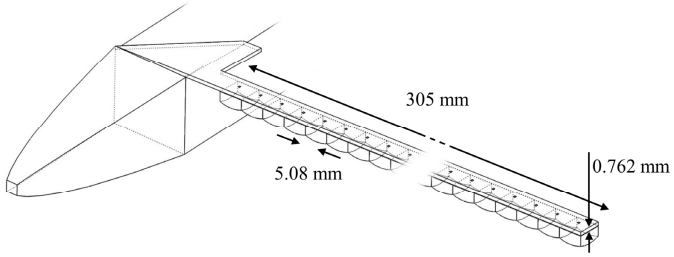

Fig. 10. Single section wireframe model of optimal CMV-F design.

The physical structure was modeled in Solidworks and imported into Zemax for ray trace analysis. The full system has a 2x2 foot aperture consisting of 120x120 lenslets and 4 source LEDs. The model consisted of a full 3 dimensional structure where rays were stored after being traced through the coupler and re-launched into the waveguide to save repetitive tracing through the coupler. A sufficient number of rays were traced to achieve ergodicity. The far field directionality was simulated as a function of lateral offset [Fig. 11(a)] and the divergence as a function of rotation about the center of the array [Fig. 11(b)]. The collimated beam can be steered ± 45° maintaining over 35% optical efficiency, and can be diverged from ± 5° to ± 60° maintaining about 43% optical efficiency. Most of the loss comes from the faceted coupler, which has a relatively large aspect ratio of $M = 22$. We see good agreement between the analytic model, which assumes a top-hat beam intensity profile characterized by ψ and φ, and the Zemax simulation in Fig. 11(a).

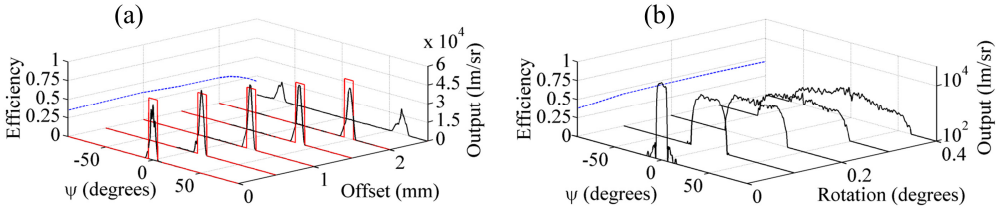

Fig. 11. Far field directivity (a) and divergence (b) simulations of the optimal CMV-F design, with total optical efficiency plotted on the left-hand plane (dashed blue). Part (a) shows good agreement between the Zemax (black) and analytic (red) models. Part (b) shows the Zemax model (black) on a log scale.

Higher efficiencies can be reached if the minimum divergence requirement is relaxed, as this enables a reduction in the aspect ratio of the coupler, an increase in waveguide thickness, and a corresponding increase in facet size. This allows coupler efficiency to be increased without reducing extraction efficiency. Similarly, relaxing the uniformity requirement increases the extraction efficiency, which also increases overall system efficiency.

#203337 - $15.00 USD Received 19 Dec 2013; revised 27 Feb 2014; accepted 15 Mar 2014; published 1 Apr 2014

3.2 Design 2: stepped mode volume with curled coupler

The second design considered uses the light coupling and waveguide structures that may be challenging to fabricate, but offer the maximum efficiency and uniformity. Based on the results of Section 2.3, we can assume nearly 100% coupling between the LED and waveguide using the curled coupler. This can be achieved for a small enough ratio of t/R independent of aspect ratio and divergence. The fixed relationship between waveguide thickness and facet geometry [Eq. (3)] allows us to write a determined set of relationships describing the geometry of the stepped structure:

$$\theta = \cos^{-1}\left(2N\left(F/\#\right)\tan\varphi\right) \tag{17}$$

$$\tan\theta = \frac{N-\cos^2\theta}{N\left(N-1\right)+\cos\theta\sin\theta} \tag{18}$$

$$t_{wg} = \frac{D\cos\theta}{N}, \tag{19}$$

where θ is the step angle of the SMV structure [Fig. 8], which decreases with increasing N.

Using Eqs. (1), (9), (12), and (19), we can express the maximum steering angle as:

$$\psi_{\max} = \sin^{-1}\left(n\sin\left(\tan^{-1}\left(\frac{1}{2\left(F/\#\right)}-\tan\left(\sin^{-1}\left(\frac{h_1 N}{\cos\theta}\sqrt{\frac{I_{out}}{\eta_{coupler}P_{LED}}}\right)\right)\right)\right)\right). \tag{20}$$

During optimization, we iterate through $\{F/\#, N\}$ space, first solving the transcendental equation defined by Eqs. (17) and (18) for φ and then for θ, then we solve Eq. (20) to determine the performance metric. Due to the fixed relationships between the waveguide and extraction feature geometries, the space is constrained to 2 dimensions [Fig. 12]. The efficiency is independent of F/# and N and is only determined by Eq. (8) and parasitic Fresnel losses which were not considered in the anaylic model.

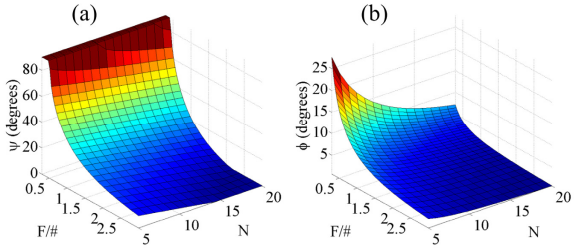

Fig. 12. SMV-C design space for 100% of the target emittance. (a) Maximum steering angle and (b) minimum beam divergence angle, constrained to $\{F/\#, N\}$ space.

This design benefits greatly from a nearly ideal coupling structure and extraction mechanism. The $1.475\text{x}10^4$ lux target emittance could be met while retaining a useful portion of the design space. We chose an optimal design with $N = 20$, $F/\# = 0.5$, and $t_{wg} = 0.761\,\text{mm}$ [Fig. 13]. Like the CMV-F design, this design also used a reflective lens array to achieve the necessary F/#. This yielded a predicted maximum steering angle of ± 60° and a minimum divergence angle of about ± 5°.

#203337 - $15.00 USD Received 19 Dec 2013; revised 27 Feb 2014; accepted 15 Mar 2014; published 1 Apr 2014

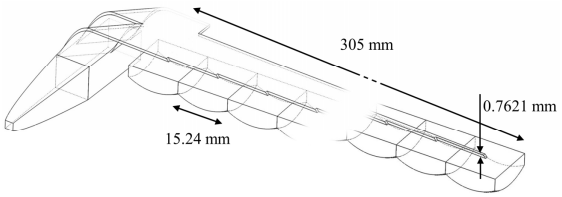

Fig. 13. Single section wireframe model of optimal SMV-C design.

The full system has a 2x2 foot aperture consisting of 40x40 lenslets and 6 source LEDs. We used the same modeling technique discussed in Section 3.1 to simulate the system performance. The result of the Zemax simulations, shown in Fig. 14, confirm that the system can steer the beam ± 60° while maintaining over 75% optical efficiency and diverge the beam from ± 5° to essentially hemispherical illumination maintaining about 80% optical efficiency. The main source of loss in this design came from Fresnel reflections. To reach higher efficiencies the optics could be anti-reflection coated, at an increased manufacturing cost.

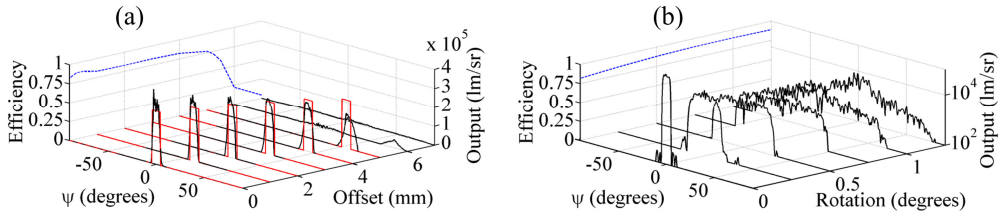

Fig. 14. Far field directivity (a) and divergence (b) simulations of optimal SMV-C design, with total optical efficiency plotted on the left-hand plane (dashed blue). Part (a) shows good agreement between the Zemax (black) and analytic (red) models. Part (b) shows the Zemax model (black) on a log scale.

A third design using a constant mode volume waveguide with a curled coupler (CMV-C) was optimized and simulated and occupied a middle-ground between the previously discussed CMV-F (35% optical system efficiency) and SMV-C (75% optical system efficiency) designs in both manufacturability and performance. The optimal CMV-C design emitted 1.22×10^4 lux and could steer the beam ± 60°, operating above 62% optical system efficiency, and could diverge the beam from ± 5° to hemispherical illumination.

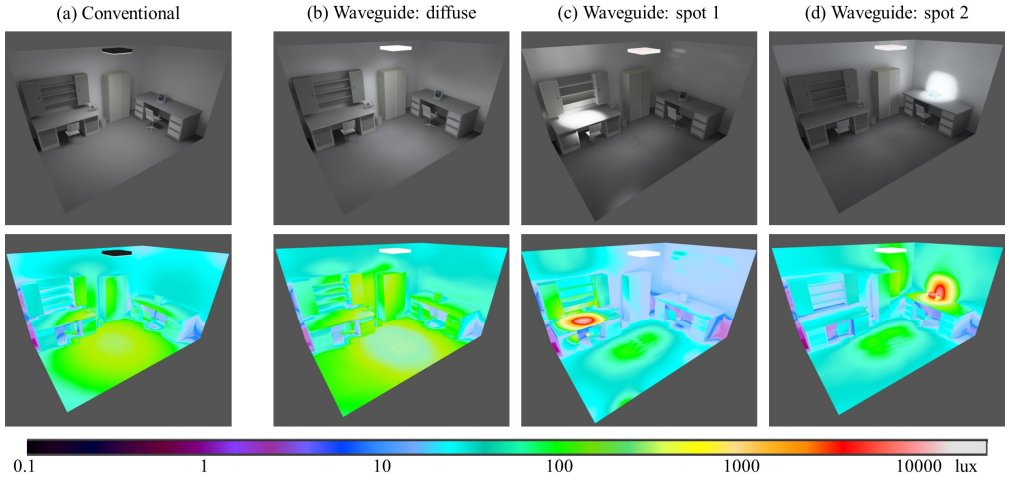

Fig. 15. Dialux simulations of conventional 2x2 foot LED fixture (a) and optimized SMV-C design (b) - (d). The waveguide system was simulated in three configurations: [diffuse] 1° rotation, [spot 1] (Δx, Δy) = (-3, 3) mm, and [spot 2] (Δx, Δy) = (5, 0) mm.

#203337 - $15.00 USD Received 19 Dec 2013; revised 27 Feb 2014; accepted 15 Mar 2014; published 1 Apr 2014

The final step in the design was to compare the overall light emission for the optimized SMV-C design to a benchmark LED troffer fixture. The far field polar intensity information for the waveguide system was exported from Zemax into Dialux [18] to simulate the illumination pattern in a realistic environment. The result is shown in Fig. 15. The conventional LED fixture [Fig. 15(a)] has a 2x2 foot aperture, consumes 53W, and produces 4000 lm with a nearly Lambertian pattern. The optimized SMV-C design [Figs. 15(b)–15(d)] also has a 2x2 foot aperture, consumes 52.84 W, but produces 4800 lm output. The waveguide design can create a similar diffuse illumination distribution [Fig. 15(b)] when configured with a 1° rotation between the lens and extraction arrays. The unique capability of the waveguide system is shown in Figs. 15(c) and 15(d), in which a collimated spot is steered to each desk in the room, producing a spot more than 10x brighter than any point in the previous two illuminance distributions. Since the LED output level can be controlled, the waveguide system can provide localized task lighting with lower energy consumption.

4. Prototype fabrication and characterization

The modeled systems in Section 3 used optimized components to achieve high system performance. To demonstrate the concept and compare model with measurement, we constructed a prototype system using commercially available or easily fabricated components. Because alignment tolerances scale with component size, the physical scale of parts was the driving factor in determining our choice of components.

We used F/1.04 refractive Fresnel lenses molded from poly methyl methacrylate (PMMA) available in 4x4 arrays measuring 3x3 inches. To reduce F/# and increase steering range we increased the lens power by stacking two lens layers for a final F/0.7 lens, measured in the PMMA waveguide. The Fresnel lenses were oriented so that the grooved sides were both facing away from the source. For the extraction features, we used 1mm diameter steel ball bearings epoxied into hemispherical recesses machined into the waveguide. The spherical symmetry of the bearings translates into relaxed alignment tolerance and a higher degree of repeatability compared to flat facets, which would require precise 3 dimensional alignment. The spatial extent of the 1mm diameter hemispheres gives a 3.2° half divergence angle of emitted light. For the waveguide, we used a 2.54 mm thick planar sheet of PMMA, where the thickness was chosen to produce uniform and efficient extraction. A 10.6 mm thick PMMA substrate was glued to the bottom of the lens array to minimize the air gap between the waveguide and lens structure while keeping the total optical distance between lens and extraction feature equal to the focal length. We found that an air gap of 100-300 μm between the lenses and waveguide was sufficient to minimize undesirable divergence, and could be achieved using a small number of thin Teflon spacers distributed across the system aperture.

The curled and faceted couplers discussed previously provide a relatively collimated and axially symmetric angular spectrum, which is ideal for use with flat facets. However, when using spherical extraction features, there is no need for the illumination to be collimated or axially symmetric due to the scattering properties of a sphere. From an étendue perspective, the spheres are more efficiently illuminated by light with a larger divergence angle and a higher spatial power density. Additionally, the extraction efficiency of spherical facets was found to increase when light propagates with a large average angle with respect to the waveguide plane, so long as the TIR condition is obeyed. Based on these observations, we used a linear array of closely-spaced 0.43 mm thick LEDs attached to a 1-D CPC to reduce the divergence in the plane normal to the waveguide while allowing full divergence in the plane of the waveguide. The CPC bar was attached to the waveguide at a 36° angle with respect to the waveguide plane. The CPC couplers were machined out of polycarbonate and vapor polished to produce a specular surface finish, and later sputtered with 1 micron thick silver reflector (measured to be >85% efficient) to increase reflectivity in regions of the CPC that were not TIR limited. The LEDs were chosen for their thin form factor, allowing adequate collimation defined by the 1-D étendue relation, and for their high flux of 4.38 lm from a 2.3x0.3 mm aperture. The LEDs were reflow-soldered onto a printed circuit board (PCB) while using an alignment fixture machined from FR-4 to register the LEDs to about

#203337 - $15.00 USD Received 19 Dec 2013; revised 27 Feb 2014; accepted 15 Mar 2014; published 1 Apr 2014

200 μm positional tolerance. This tight alignment tolerance allowed efficient interface with the CPC coupler.

4.1 Unit cell device

Prior to fabrication of a full 2x2 foot aperture system, we constructed a 'unit cell' consisting of a waveguide with a single 1 mm hemispherical extraction feature, a small section of the lens array, and 3 LEDs [Fig. 16(a)]. The lens array was mounted onto a 3-axis translation stage for accurate positioning relative to the waveguide. The far field intensity pattern was measured 1 meter from the lens aperture. The intensity pattern is a superposition of 3 patterns from the 3 LEDs, with some fine structure because the coupled waveguide modes had not fully homogenized before striking the facet. An equivalent system was modeled in Zemax and its corresponding far field pattern shows excellent agreement with measurement [Fig. 16(c)].

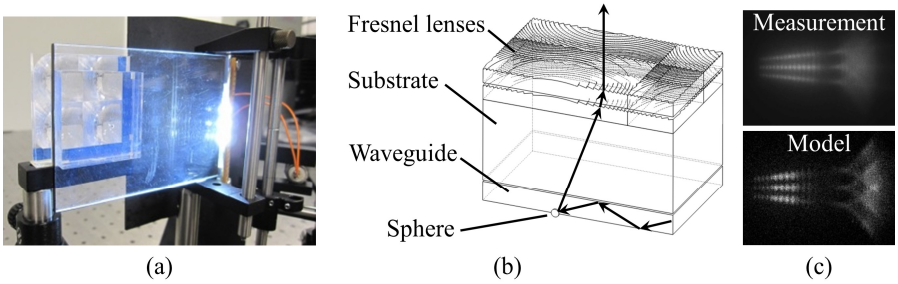

Fig. 16. (a) Unit cell system. (b) Cut-away schematic drawn to scale and illustrative ray path. (c) Measured (top) and simulated (bottom) far field intensity patterns.

The unit cell system was also used to characterize the directional capabilities of the system by taking intensity line scans 1 meter from the aperture for different lateral offsets between the lens array and extraction feature [Fig. 17]. The data is plotted against curves from a corresponding polar far field Zemax simulation of a full 2x2 foot aperture system (black) and a modified semi-analytic version of the CMV model discussed in Section 3.1 (red). The measured data (blue) is scaled to arbitrary units because the output power of the full aperture system cannot be directly inferred from the unit cell device. We also cannot determine the divergence capabilities because only one lens/extraction feature pair is present. We see relatively good agreement between both models and measurement, with the exception that the measured off-axis intensity falls dramatically compared to either model. The attenuation is significant at high field angles and completely eliminates the crosstalk lobe seen in both the analytic and Zemax models. This inconsistency can be explained by the poor off-axis Fresnel lens performance compared to the ideal paraxial lens used in both models.

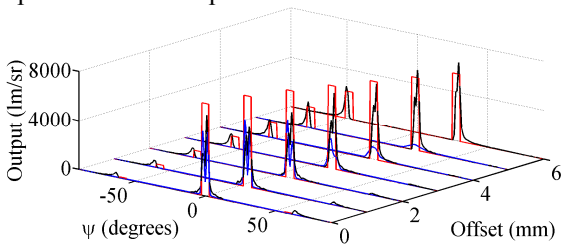

Fig. 17. Far field directivity of the unit cell system: analytic model (red), Zemax simulation (black), and lab measurement (blue). Measured drop in off-axis intensity is due to poor off-axis lens performance.

4.2 Full aperture system

Next we fabricated a full 2x2 foot aperture prototype composed of a 26x26 element extraction array and 28x28 lens array, both with a 19mm pitch, and 304 source LEDs. The lens array was larger than the extraction array to prevent clipping at the corners during rotation. Light

#203337 - $15.00 USD Received 19 Dec 2013; revised 27 Feb 2014; accepted 15 Mar 2014; published 1 Apr 2014

was coupled into the waveguide from two edges, allowing room for mechanical control from the opposite edges. We attached high strength neodymium magnets to the lens array at 3 points on the edges opposite to the sources and used ferromagnetic eccentric cams seated on the magnets to translate and rotate the lens array relative to the extraction array. Rotation of the cam through a 180° angle produced the 20 mm travel required for opertation. Our prototype used manual control, but could easily be fitted with motorized controllers to enable remote electrical operation. The computer-aided-design (CAD) model as well as the physical realization of the system components and fully assembled system is shown in Fig. 18.

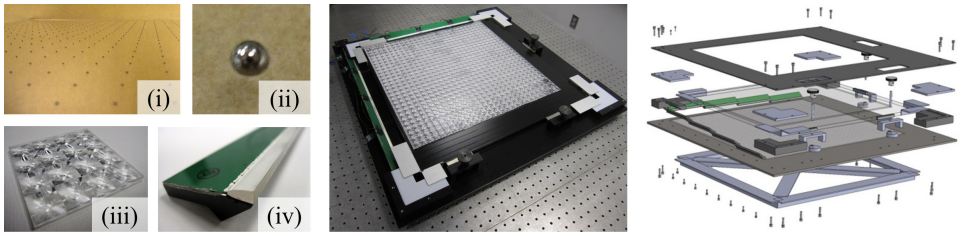

Fig. 18. (a) System components: (i) waveguide, (ii) ball-bearing extraction feature, (iii) lenses, and (iv) PCB, LEDs, and CPC coupler; (b) assembled system (shown without cover); and (c) exploded CAD model.

Qualitative [Fig. 19] and quantitative [Fig. 20] measurements were taken 3 meters from the system aperture using a camera and calibrated photodiode, respectively, demonstrating good agreement with both the semi-analytic and Zemax models. The top-hat profile beam calculated with the semi-analytic model was mapped from polar far field space to physical space using simple radiometric calculations. The scattering of light from Fresnel zone transitions accounts for the main discrepancy between model and measurement. From lens cross section measurements the zone transitions were estimated to obscure about 30% of the clear lens aperture, accounting for the reduction in central beam power and resultant increase in the noise pedestal surrounding the beam. This effect becomes more pronounced as the beam is steered to more extreme angles. This also explains the behavior observed for extreme rotations, where we find the system acts more like a diffuse emitter instead of preferentially 'spreading out' the light according to the Zemax model.

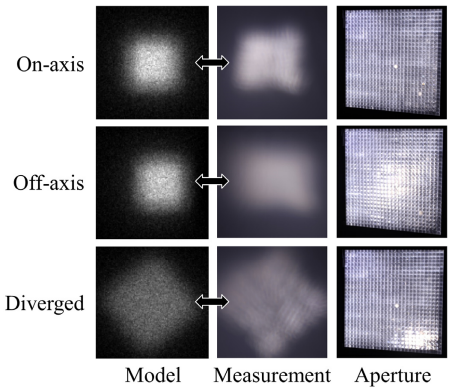

Fig. 19. Simulation (left column) and measurement (center column) of on-axis, off-axis, and diverged spots 3 meters from the aperture. The right column shows the corresponding view of the aperture from an angle.

Polar integration of the illuminance line scan measurements yields a total output of 98 lm, corresponding to an optical system efficiency of 7.6%, which agrees well with the simulated optical efficiency of 7.56%. The major source of loss in the prototype came from the high absorption coefficient of the PMMA waveguide, measured and simulated to be 0.5 m^{-1}. Zemax simulations showed that using a BK7 waveguide with an absorption coefficient of

#203337 - $15.00 USD Received 19 Dec 2013; revised 27 Feb 2014; accepted 15 Mar 2014; published 1 Apr 2014

$3x10^{-4}$ m^{-1} (used in the optimized theoretical designs) would increase the overall optical system efficiency of the prototype to 31%. Secondary sources of loss in the prototype were coupling mirror loss, waveguide surface scattering, and small misalignments in the couplers and lens array. While the prototype system is highly inefficient compared to optimal designs, the consistency between measurement, model, and simulation indicates that the predicted high efficiencies for optimized designs [Table 1] are credible. This agreement also supports the accuracy of the analytic model in representing the system during design and optimization.

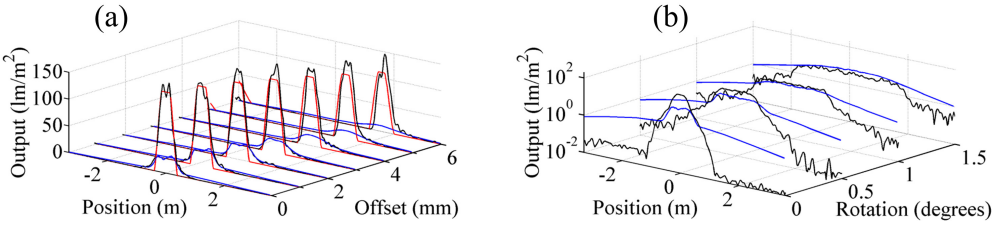

Fig. 20. Near field directionality (a) and divergence (b) of the prototype system 3 meters from the aperture. Part (a) shows the analytic model (red), Zemax model (black), and measurements (blue). Part (b) shows the Zemax model (black) and measurement (blue) on a log scale.

Table 1. System Efficiencies and Loss Mechanisms

Design	System efficiency	Dominant sources of loss
SMV-Curled	75%	Fresnel reflections from uncoated interfaces
CMV-Curled	62%	+ Imperfect extraction in the CMV waveguide
CMV-Faceted	35%	+ Suboptimal coupler efficiency
Lab prototype	7.6%	+ Large material absorption of PMMA waveguide

5. Conclusion

We showed how a planar waveguide illuminator with periodically patterned extraction features and lens array can be used to control both the directionality and divergence of light output using short-range mechanical motion.

The system performance depends on a large number of variables, which led us to develop an analytic model compatible with the two coupling and two waveguiding designs considered in order to perform system-level optimization. The analytically optimized designs were ray traced in Zemax and the resulting performance was in good agreement with the analytic model. We found that the optimal design used a stepped mode volume glass waveguide and curled coupler. This design could steer a collimated beam over ± 60° and diverge the beam from ± 5° to fully hemispherical illumination, while maintaining over 75% optical efficiency, for a total output of 4800 lumens from a 2x2 foot aperture.

We constructed a proof-of-principle prototype from commercially available components which successfully demonstrated both the beam steering and diverging principle in a 2x2 foot aperture embodiment. Although the optical efficiency of the device was only 7%, good agreement between the measurement, Zemax simulation, and analytic model was established, supporting the predictions of high efficiency and high output power in optimal designs which used fully custom optical components. The next step would be to fabricate an efficient system using the optimized optical structures, and using electrical controllers to allow remote actuation.

In future research, the same basic concept could be extended to provide a thin energy efficient flat panel display where light energy is actively directed toward one or more users, whose position may be tracked using a video camera and face-tracking software. Given accuracy sufficient to selectively illuminate each of the user's eyes, this approach may be used for multi-user glasses-free 3D display.

Acknowledgments

This research was made possible with support from CogniTek. The authors would also like to thank Dr. Ilya Agurok for helpful discussions.